metals

MDPI

Article

Analysis of the Effects of Water Temperature on Water-Assisted Laser Trepanning in Superalloys

Kaibo Xia [1,2,*], Liang Wang [3], Mingchao Li [1] and Huayu Yang [1]

[1] School of Mechanical Engineering, Jiangsu University, Zhenjiang 212013, China
[2] Suzhou Delphi Laser Co., Ltd., Suzhou 215026, China
[3] Faculty of Mechanical and Materials Engineering, Huaiyin Institute of Technology, Huaian 223000, China; wangliang@hyit.edu.cn
* Correspondence: xiakaibo@ujs.edu.cn

Abstract: The water-assisted laser trepanning method has been proven to improve the quality of laser drilling; however, the effect of water temperature on this process is currently unclear. In order to investigate the influence of water temperature on the quality of holes produced via water-assisted laser trepanning in superalloys, this study used the controlled variable method to investigate the effects of three water temperatures—low temperature (2 °C), normal temperature (20 °C), and high temperature (70 °C)—on the following factors: spatter, hole diameter, taper angle, hole sidewall morphology, and recast layer. The results show that the spatter around the hole reduced, the hole entrance/exit diameter increased, and the roughness of the hole's sidewall decreased with an increase in single-pulse energy. However, the effect of single-pulse energy on the recast layer was not obvious. As the temperature of the water increased, the hole entrance/exit diameter increased, and the roughness of the hole's sidewall decreased. When the single-pulse energy was 1.0–1.9 J, using a lower water temperature produced a hole with a smaller taper angle. Compared with a water temperature of 20 °C, the movement of the melt film on the hole's sidewall accelerated when the water temperature was 70 °C; as a result, more molten material could be removed from the hole, resulting in a decrease in the thickness of the recast layer. However, when the water temperature was 2 °C, the heat-affected zone and the thickness of the recast layer decreased more significantly. The results of this study provide technical support for the optimization of water-assisted laser drilling.

Keywords: superalloy; laser trepanning; water assistance; water temperature; single-pulse energy

Citation: Xia, K.; Wang, L.; Li, M.; Yang, H. Analysis of the Effects of Water Temperature on Water-Assisted Laser Trepanning in Superalloys. *Metals* **2024**, *14*, 943. https://doi.org/10.3390/met14080943

Academic Editor: Thomas Niendorf

Received: 30 June 2024
Revised: 1 August 2024
Accepted: 17 August 2024
Published: 19 August 2024

1. Introduction

Laser drilling, as a non-traditional processing method [1], has the advantages of high processing precision [2], no loss of tools [3], and high drilling efficiency [4], among others. Laser drilling has gradually replaced other traditional processing methods and become a research focus in the field of microhole processing [5]. However, with the rapid development of industry, market demand for high-quality and efficient microhole drilling methods is gradually growing [6]. Therefore, determining how we might improve the efficiency of laser drilling operations [7], increase aspect ratios [8], and reduce recast layers [9] and microcracks [10] is a focus of many researchers [4].

Relative to laser percussion drilling, laser trepanning can achieve holes with improved morphology [11]. Wang et al. [12] used a femtosecond laser to process gas film cooling holes with K24 superalloy; they compared three different scanning paths and eventually chose a laser multi-layer scanning method. Their research results indicated that when the average power was high, the scanning speed was low, the feed distance was small, and the scanning time was moderate, higher-quality holes were produced. Saini et al. [13] used a millisecond laser to perform trepanning on ZTA ceramics and studied numerical changes in microcracks, recast layers, and microhardness on the hole's sidewall. They did

so by changing the parameters of their process. Such experiments have found that when the laser pulse width is low and the cutting speed is slow, selecting a higher assisted gas pressure reduces the width of microcracks on the hole sidewall and the thickness of the recast layer. Jia et al. [14] selected alumina ceramics as their experimental material and used nanosecond pulses in the initial sequence before incorporating millisecond pulse sequences to create a novel combined pulse laser processing technology (CPL). Their experimental results indicated that the small holes on the workpiece, ablated by the initial nanosecond pulse, help to increase the energy absorption of the material using subsequent millisecond pulses, thereby resulting in better drilling quality. At the same time, increasing the rate of the repetition of subsequent nanosecond pulses significantly improved the quality of holes. In order to address the relationship between system layout, laser beam direction, and hole geometry in laser trepanning, Ye et al. [15] proposed a universal model of the commonly used four-wedge trepanning system. This model was able to analyze the motion trajectory of the laser beam during drilling and, in doing so, could predict the geometric shape of the hole. The simulation results were compared and verified with the experimental results. Zhang et al. [16] applied machine learning to the establishment of a laser drilling prediction model, improving the speed and accuracy of the model to circumvent a significant amount of experimental work. On the basis of this model, they further optimized the laser drilling prediction model by combining it with a genetic algorithm.

In recent years, relevant research has shown that water-assisted laser drilling can effectively reduce defects such as heat-affected zones, recast layers, and microcracks, further improving the quality of the microhole produced [17]. Zhu et al. [18] proposed a water-assisted laser drilling method in order to address issues such as severe substrate thermal deformation, large hole tapering, and poor consistency in hole shapes during the laser drilling of metal filters. The experimental results show that, when using the same processing parameters, the water-assisted method can reduce hole tapering, the thickness of the recast layer, and the heat-affected zone range (when compared with the conditions of ambient air). Finally, optimal process parameters were determined using orthogonal experiments. Chen et al. [19] studied the effects of the laser scanning speed and processing environment on the tapering of holes produced via underwater laser drilling. The results indicated that underwater drilling had a greater impact on the tapering of holes than laser drilling in the air. A method for calculating variation in hole tapering along with variation in hole depth has been proposed as a means of describing hole shape during underwater laser drilling. In order to effectively improve the drilling quality of yttria-stabilized zirconia (YSZ), Feng et al. [20] conducted experimental research on ultrafast laser drilling in an underwater environment. Multi-objective optimization methods were used, and the influence of parameters such as laser power, defocus amount, scanning speed, and scanning cycles on the geometric quality of holes was systematically studied. As a result, optimal process parameters were obtained. Wang et al. [21] used a 515 nm wavelength femtosecond laser to drill holes in 4H-SiC materials in air and underwater, respectively. After drilling in air, large areas of cracking, surface material detachment, a recast layer, and a heat-affected zone were observed; such features were not observed after water-assisted laser drilling. In order to obtain optimal process parameters, the effects of repetition frequency, water film thickness, and focal position on the quality and efficiency of laser drilling were studied. Zhang et al. [22,23] proposed a two-step machining strategy based on through-hole drilling and modification, and they studied the effects of pulse energy, scanning speed, pulse frequency, and modification numbers on the geometry of holes. Finally, a hole with good roundness and a small amount of tapering was obtained.

In summary, laser drilling with water assistance can improve the results achieved, but few relevant studies have examined this method; moreover, there is limited research on the differences between various water-assisted laser drilling approaches. We researched different water-assisted methods for laser drilling in our preliminary work, and the results indicated that the best hole quality was achieved using a water-assisted laser drilling method (the water surface was set at the same height as the upper surface of the workpiece).

However, the effect of water temperature is currently unclear. In this study, in order to investigate the effects of water temperature on the quality of holes produced via water-assisted laser trepanning in superalloys and provide technical support for the optimization of the water-assisted laser drilling process, GH4220 nickel-based superalloy was selected as our experimental material. The effect of water temperature on the quality of millisecond laser trepanning was investigated using the water-assisted laser trepanning method, and the effects of single-pulse energy on the spatter, hole entrance/exit diameter, taper angle, hole sidewall morphology, and recast layer were analyzed.

2. Materials and Methods

GH4220 nickel-based superalloy (Dongguan Tengfeng Metal Materials Co., Ltd., Dongguan, China) was used in this experiment. This alloy has good comprehensive strengthening performance and is well suited to producing rotating components, such as turbine blades for aircraft engines, which operate in a high-temperature environment of 950 °C. Its chemical composition can be found in Reference [24]. The density of GH4220 superalloy is 8.36 g/cm^3, and its melting point range is from 1330 to 1360 °C. The specific heat capacity and thermal conductivity of the material at different temperatures are shown in Table 1.

Table 1. Thermophysical parameters of GH4220 nickel-based superalloy data from [24].

Temperature/°C	100	200	300	400	500	600	700	800	900
Specific heat capacity/J·kg^{-1}.°C^{-1}	472.3	473.1	473.5	473.9	475.2	476.9	477.3	481.1	484.0
Thermal conductivity/W·m^{-1}.°C^{-1}	9.6	11.3	12.6	14.7	15.9	18.0	19.7	21.4	23.5

Prior to conducting the experiment, the workpiece was prepared. Firstly, a GH4220 superalloy rod with a diameter of 30 mm was cut into circular pieces of the same thickness using a wire-cutting method, and a small amount of material was retained to provide an allowance for grinding and polishing (0.1 mm allowance). Detergent was used to remove residual oil stains on the surface of the workpiece during the wire-cutting process. Subsequently, a metallographic polishing machine combined with water sandpaper was used to remove scratches left by the wire-cutting procedure. During the grinding process, the thickness of the workpiece was continuously measured using a Vernier caliper to ensure that the final thickness met the requirements. Finally, the workpiece was cleaned with an ultrasonic cleaning machine for 5 min (using anhydrous ethanol as the cleaning agent). A 1.6 ± 0.1 mm superalloy workpiece was used in the experiment. We selected this particular thickness as it is the industry standard for the machining of film cooling holes for aircraft engine turbine blades, i.e., the context in which we performed this study. The range of the film cooling holes' depth on the blades is usually from 1 to 6 mm [25]. In this study, we selected a depth of 1.6 mm, which is well within this industry-standard range.

During laser trepanning, the workpiece remains stationary while the laser head moves in a circular motion on a horizontal plane, as shown in Figure 1a. The laser drilling equipment used in this study was the DMG LASERTEC 80 PowerDrill (Jiangsu University, Zhenjiang, China), which is produced by the DMG corporation in Stuttgart, Germany. The laser parameters can be found in Reference [26]. Compared with laser precision, laser trepanning can better control the resulting hole shape and diameter. Therefore, for this experiment, we adopted the water-assisted laser trepanning method. The water surface was set at the same height as the upper surface of the workpiece, as shown in Figure 1b. We then studied the effect of water temperature on the water-assisted millisecond laser trepanning method. In the experiment, 0.1 MPa of argon was used for coaxial blowing. The experimental parameters are listed in Table 2.

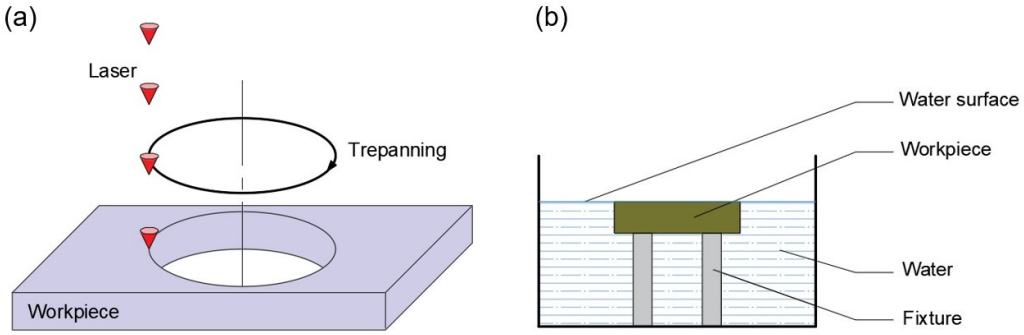

Figure 1. Schematic diagram of the water-assisted millisecond laser trepanning method: (**a**) scanning path; (**b**) water-assisted laser drilling.

Table 2. Laser parameters used in water-assisted laser trepanning experiments with different temperatures.

Case	Pulse Width (ms)	Pulse Repetition Rate (Hz)	Single-Pulse Energy (J)	Number of Circles	Scanning Speed (mm/min)	Water Temperature/°C
I	0.8	60	0.7–1.9	2	50	2
II	0.8	60	0.7–1.9	2	50	20
III	0.8	60	0.7–1.9	2	50	70

In this experiment, control over the water temperature was achieved via two methods (the heating and cooling of the water), which were carried out with a low-power electric heating rod/semiconductor cooling fin. The water temperature was monitored through an electronic display thermometer fixed outside the tank. Before the experiment, the water was heated or cooled to a temperature close to the experimental requirements and then injected into the tank. Then, the water temperature was adjusted to the required temperature using a water temperature control system, and the temperature was kept as constant as possible during the experiment. After one drilling experiment was completed, we repeated the above steps to adjust the water temperature to the temperature required for subsequent experiments.

After the experiment, the diameters of the hole entrance and exit were measured using KEYENCE confocal laser scanning microscopy (CLSM, which was produced by the KEYENCE corporation in Osaka, Japan and performed at Jiangsu University, Zhenjiang, China), with a difference of 30° between each measurement. The average of the six values was calculated to avoid measurement errors and produce values that were as realistic as possible [26]. Then, the taper angle was calculated [26]. Next, the hole's cross-section was created by grinding and polishing, and the cross-sectional morphology and sidewall morphology were observed using CLSM. Finally, the recast layer was characterized and measured using CLSM after chemical etching. In order to improve the reliability of the experimental analysis, the experiment was repeated three times, and the average value of the three experiments was used for data analysis.

The surface roughness of the hole sidewall was measured using CLSM analysis software (MultiFileAnalyzer 1.3.1.120). The surface roughness (S_a) is the average absolute height value of each point in the defined area, and it may be calculated as follows:

$$S_a = \frac{1}{A}\iint_A |z(x,y)|\mathrm{d}x\mathrm{d}y \quad (1)$$

In the formula, z (x, y) is the height of a point on a plane with an area of A.

3. Results and Discussion

3.1. Spatter

Figure 2 shows the spatter around the hole's entrance at different water temperatures. An area of oxidation was observed around the hole's entrance. When the hole was drilled through, water entered the hole, and the material surface was heated and cooled unevenly under the influence of both laser and water; therefore, some areas of oxidation were generated. When the single-pulse energy was low, more spatter occurred around the hole entrance, and large-scale oxidation patterns were observed. When the energy was low, the molten material could not be removed from the hole in time, resulting in residue around the hole's entrance. We also observed that when the water temperature was 70 °C, the spatter around the hole entrance was slightly less pronounced than in experiments with the other two water temperatures. This reduction in spatter occurred because, when the water temperature was high, the flushing effect of the water medium on the hole sidewall was more pronounced during laser processing, and the evaporation effect was more intense, resulting in greater removal of molten materials and debris. In addition, when the spatter was exposed to more water and water vapor, it could not readily remain on the surface around the hole entrance. Due to coaxial blowing, significant spatter accumulated at the hole's exit, but this could not be observed using a microscope. Therefore, in this study, we did not analyze the morphology of the hole's exit.

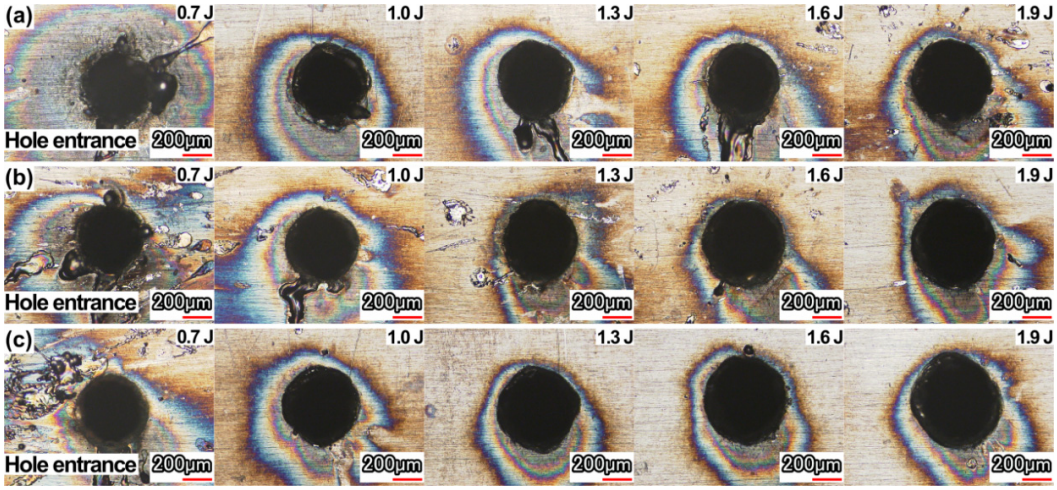

Figure 2. Effect of single-pulse energy on spatter at the entrance of microholes at different water temperatures: (**a**) 2 °C; (**b**) 20 °C; and (**c**) 70 °C.

3.2. Hole Diameter

Figure 3 shows the morphology of the hole's entrance and exit after grinding and polishing. Figure 4 shows the influence of single-pulse energy on the diameter of the hole's entrance and exit. We observed that as the temperature of the water medium increased, the hole's diameter increased (that is, when all other laser parameters were kept constant). This increase in the hole diameter occurred because, when the water temperature reached 70 °C, the evaporation of the water was more pronounced. Therefore, during laser processing, an increased amount of water vapor and water medium became involved in the process of drilling the hole. The movement of molten materials, debris, and plasma generated by the laser was accelerated; thus, the rate at which material was removed actually improved. When the water temperature was 2 °C, the lower temperature enabled the water vapor to condense into small water droplets more readily. The diffusion speed of the water vapor and metal vapor decreased, and the movement of material debris and molten material generated by the laser decreased, resulting in a decrease in the material removal rate.

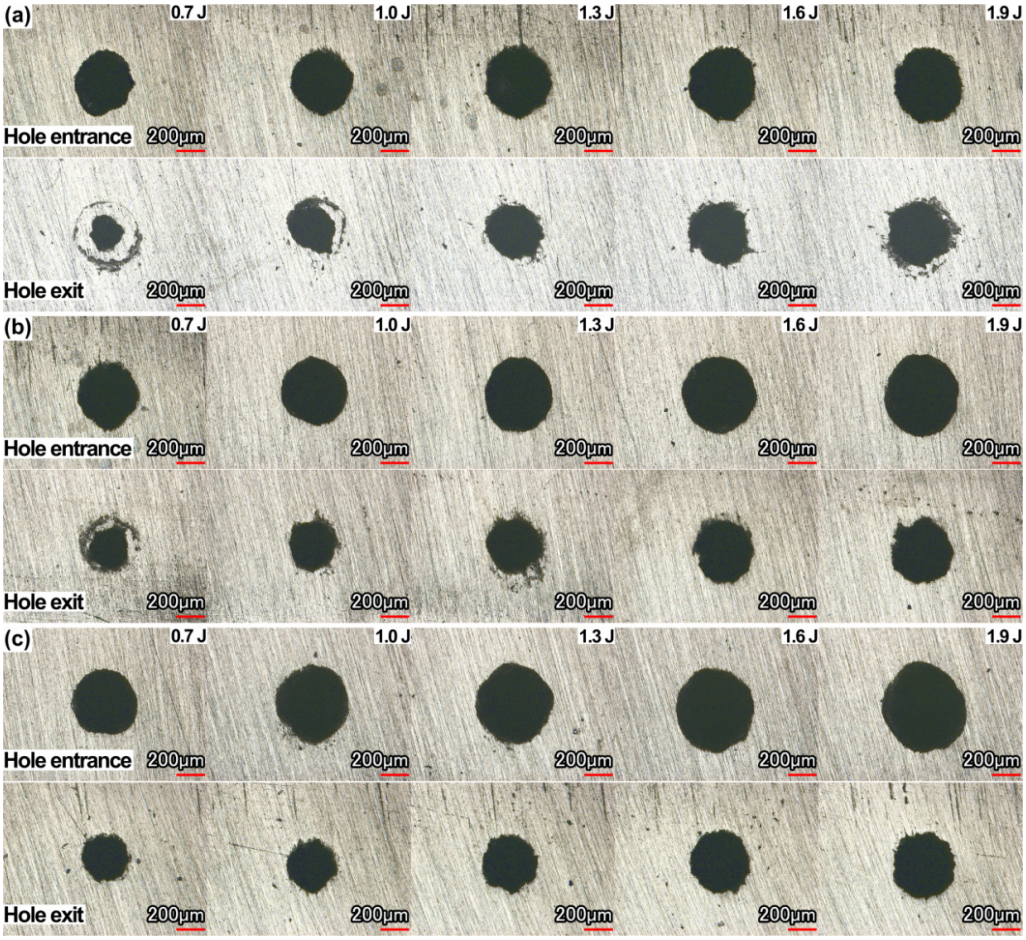

Figure 3. Effect of single-pulse energy on the morphology of microholes' entrance and exit at different water temperatures: (**a**) 2 °C; (**b**) 20 °C; and (**c**) 70 °C.

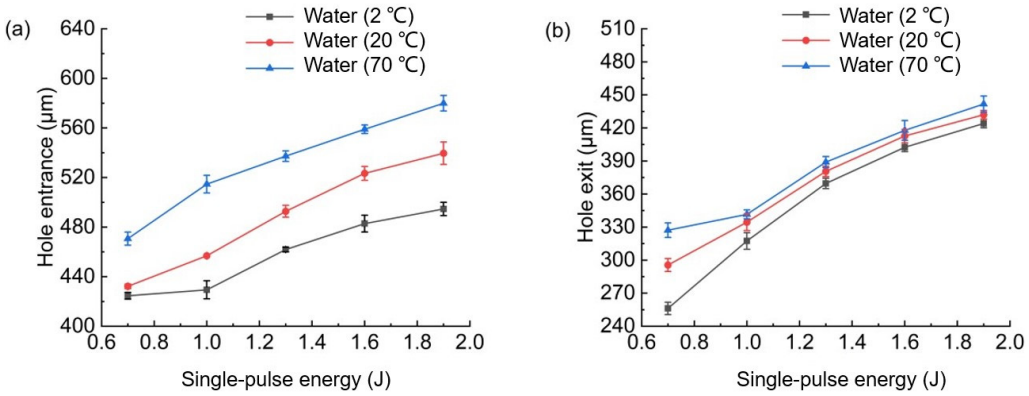

Figure 4. Effect of single-pulse energy on microhole diameters: (**a**) hole entrance; (**b**) hole exit.

3.3. Hole Cross-Section Morphology and Taper

The morphology of hole cross-sections at different temperatures with water assistance is shown in Figure 5. The increase in water temperature improved the rate at which laser materials were removed. With the increase in single-pulse energy, the material removal rate increased at various temperatures.

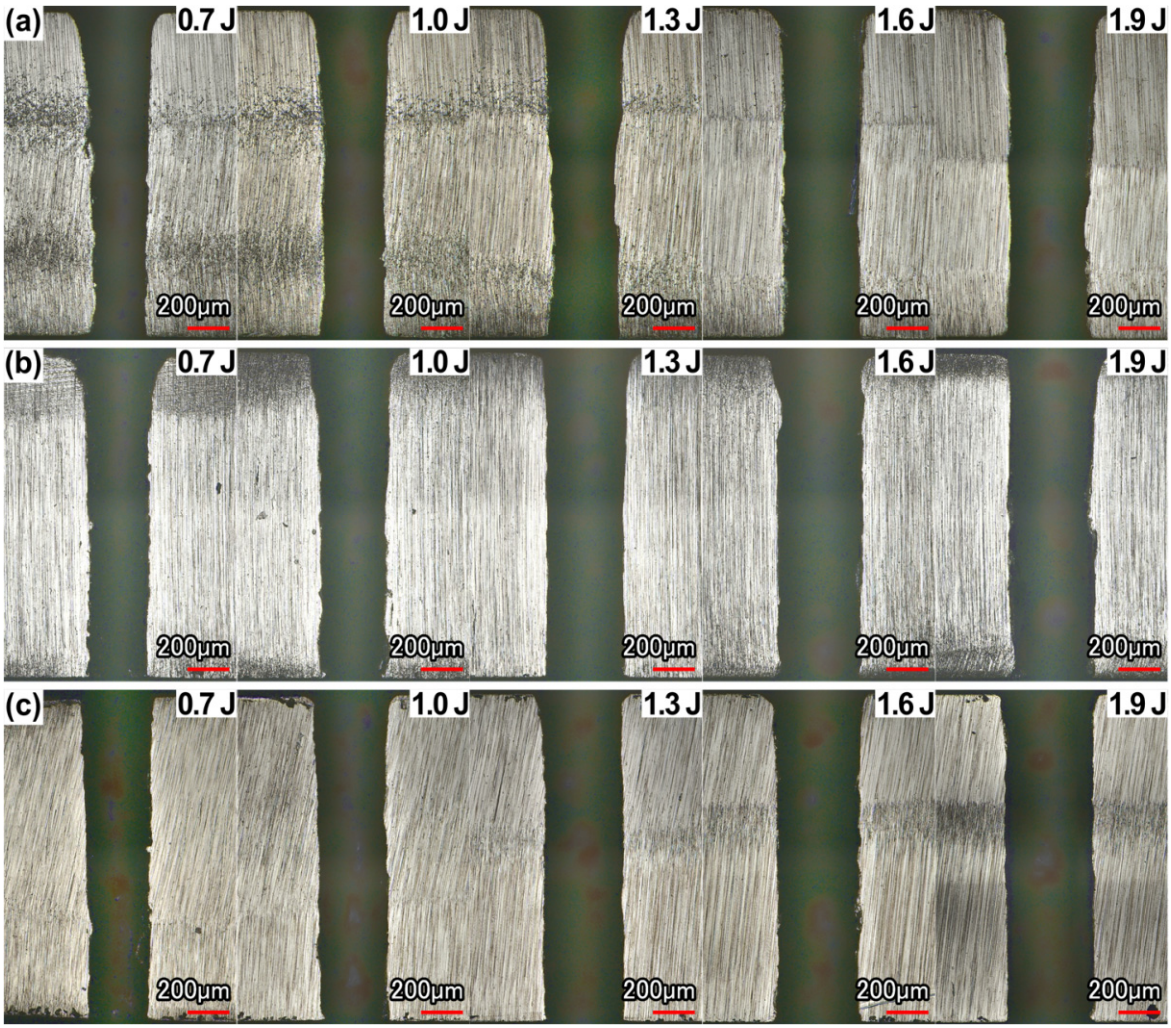

Figure 5. Effect of single-pulse energy on the hole cross-section morphology at different water temperatures: (**a**) 2 °C; (**b**) 20 °C; and (**c**) 70 °C.

Figure 6 shows the variation in tapering angle with the increase in single-pulse energy at three different water temperatures. When the single-pulse energy was 0.7 J, the hole's taper angle was highest in 2 °C water and lowest in 20 °C water. This variation was analyzed in conjunction with Figure 4.

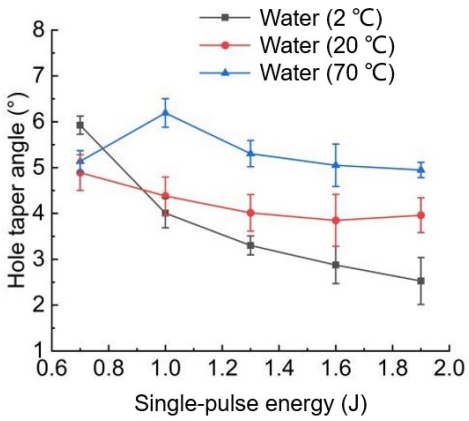

Figure 6. Effect of single-pulse energy on microholes' taper angles.

When the single-pulse energy was low, the time taken for a hole to be drilled was longer, and the time required for the water to participate in the laser drilling process was relatively short compared with other pulse energies. The water vapor generated by heating was relatively minimal, mainly affecting the hole's exit area. When the water temperature was 70 °C, the evaporation of water was more intense. At 70 °C, the water vapor provided more power for the removal of material debris and molten materials than at the other two set temperatures. With lower single-pulse energy, the material removal rate at the hole exit improved more significantly. Nevertheless, such a low temperature suppressed the diffusion of water vapor, plasma, and metal vapor, resulting in a large difference in the diameters of holes' exits at all three water temperatures when the single-pulse energy was 0.7 J.

When the single-pulse energy increased, the workpiece drilled through faster, and the participation of the water in laser drilling increased in duration. This higher pulse energy heated the water for a longer time, and more water vapor was generated. At this time, the influence of water on the hole's exit area was not as obvious as when the single-pulse energy was low. The difference between the holes' exit diameters was reduced. The increase in water temperature had a more significant impact on the diameter of the hole entrance, resulting in an increased taper angle in holes when the single-pulse energy was 1.0–1.9 J.

3.4. Roughness of the Hole Sidewall

The morphology of the hole sidewall near the entrance, middle, and exit areas of the hole was observed using CLSM at different water temperatures, with a single-pulse energy of 0.7 J (Figure 7). In 70 °C water, the traces left by the microjet generated by the water medium during processing were more obvious near the middle and exit areas of the hole sidewall.

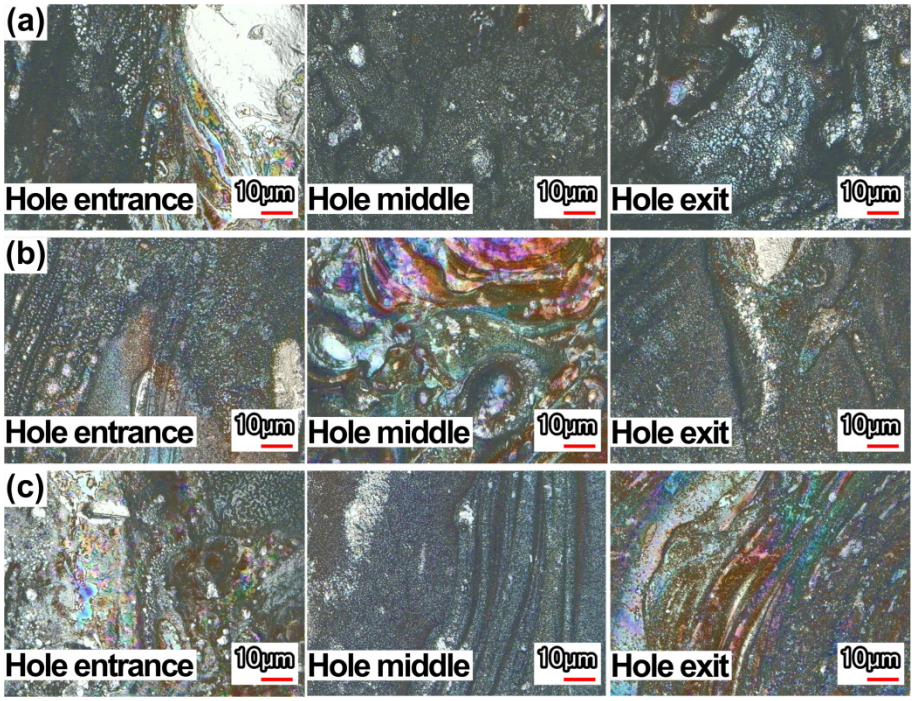

Figure 7. CLSM 2D morphology of different areas on the hole sidewall at different water temperatures: (**a**) 2 °C, (**b**) 20 °C, and (**c**) 70 °C.

Figure 8 shows the 3D morphology and roughness of the hole sidewall, corresponding to Figure 7. As the water temperature increased, the roughness of the hole sidewall decreased. This decrease in roughness occurred because when the water temperature increased, the water flow and the water vapor produced by this heating promoted the removal of molten materials and debris from inside the hole, resulting in a smoother

sidewall. However, when the water temperature was 2 °C, the roughness of the sidewall near the hole's middle and exit areas was relatively more pronounced. The reason for the increased roughness is that the lower the water temperature, the faster the cooling speed of the hole sidewall, and the more likely the hole sidewall is to produce defects such as microcracks, leading to an increase in roughness. Looking at the hole's entrance area, the temperature of the water medium increased after heating by the laser; thus, the cooling rate of the hole sidewall decreased, resulting in a decrease in roughness.

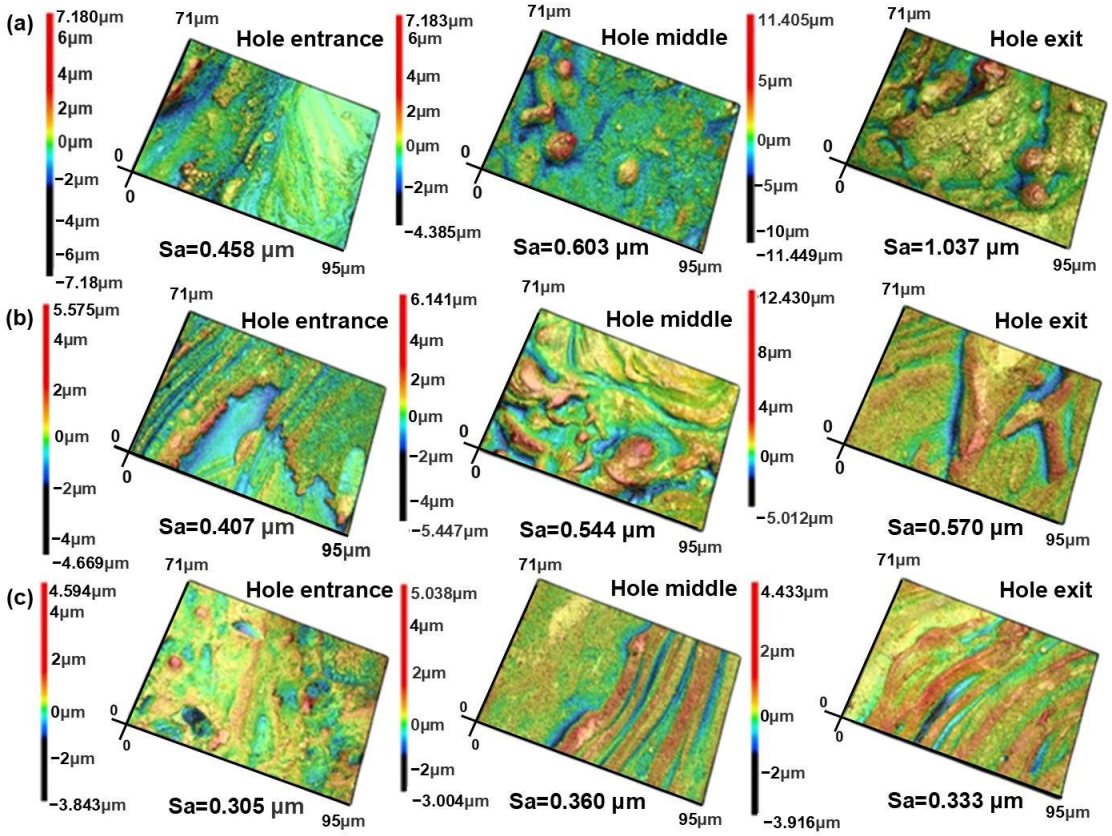

Figure 8. CLSM 3D morphology of different areas of hole sidewall at different water temperatures: (**a**) 2 °C, (**b**) 20 °C, and (**c**) 70 °C.

The 2D morphology of the middle area of the hole at different temperatures, considering the use of water assistance and a single-pulse energy of 1.9 J, is shown in Figure 9. It can clearly be seen in the figure that the microcracks inside the hole and the traces of microjet erosion are due to the rapid cooling rate at low water temperatures.

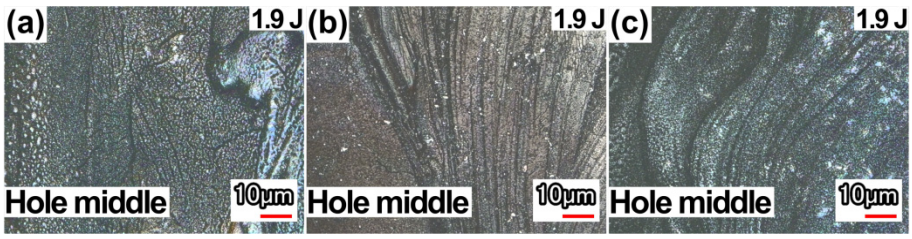

Figure 9. CLSM 2D morphology of the middle of the hole wall at a single-pulse energy of 1.9 J and various temperatures: (**a**) 2 °C; (**b**) 20 °C; and (**c**) 70 °C.

The effect of single-pulse energy on the roughness of different areas of the hole sidewall is shown in Figure 10. As the single-pulse energy increased, the roughness of the hole

sidewall decreased under all three temperature conditions. At the same time, when the water temperature increased, the roughness of different areas of the hole sidewall decreased; as a consequence, the hole quality improved.

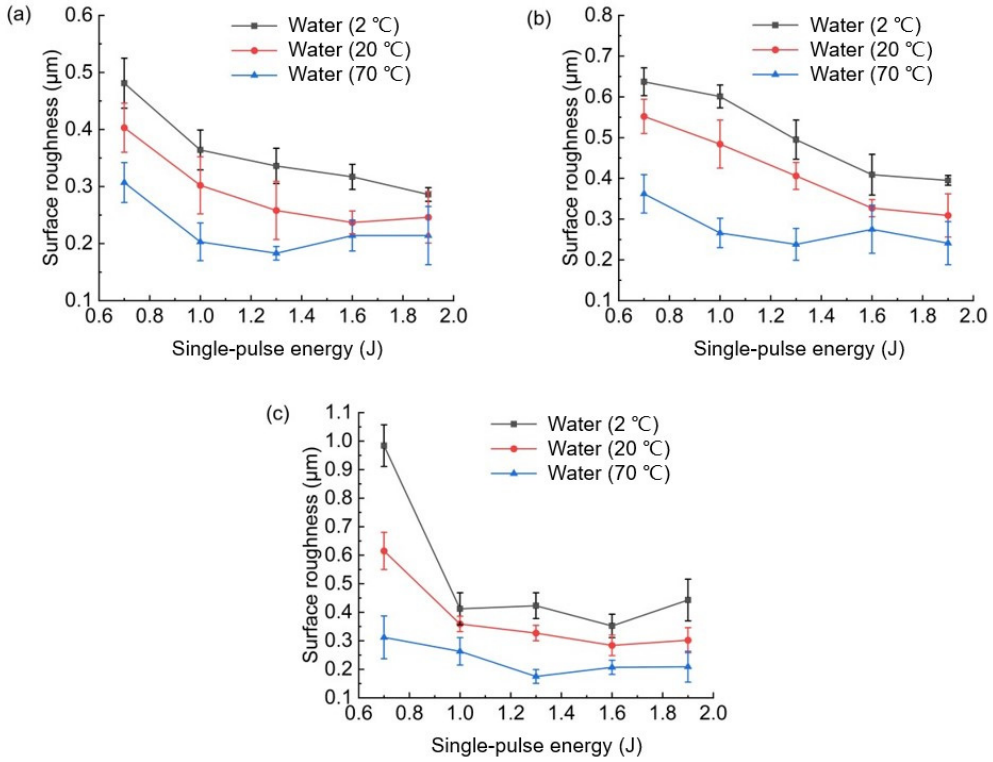

Figure 10. Effect of single-pulse energy on the roughness of different areas on the hole sidewall: (**a**) hole entrance; (**b**) hole middle; and (**c**) hole exit.

3.5. Recast Layer

The thickness of the recast layer at different locations within the hole at three set water temperatures and a constant single-pulse energy of 0.7 J are shown in Figure 11. When the water temperature was 2 °C, the recast layer on the hole sidewall was relatively thin. Under these conditions, a lower water temperature reduced the thermal impact generated during processing. Less molten material was produced inside the hole, and the recast layer that formed on the hole sidewall was also relatively thin. When the water temperature was 70 °C, the recast layer on the hole sidewall was slightly thinner than in 20 °C water. Theoretically, a higher water temperature would increase the thermal impact during laser drilling, resulting in more melt film on the hole sidewall. However, a higher-temperature water medium would also be more likely to evaporate and produce water vapor. At the same time, more bubbles were generated by heating, and the shock wave and microjet generated during bubble explosion and upward floating were more effective. Molten materials and debris could be removed from the hole and sprayed out from the hole entrance, resulting in less melt film on the hole sidewall and a decrease in the thickness of the recast layer.

The effect of single-pulse energy on the thickness of the recast layer on the hole sidewall at different water temperatures is shown in Figure 12; said effect was found to be non-significant. When the water temperature was 20 °C, the recast layer on the hole sidewall reached its highest thickness, followed by 70 °C; the recast layer was thinnest at 2 °C. Relative to the 20 °C water temperature, the lower water temperature reduced thermal impact during laser trepanning, thereby reducing the residual molten material present on the hole sidewall. The higher water temperature increased the power with which the water medium and vapor moved inside the hole, causing more molten materials to be removed

and the melt film on the hole sidewall to be reduced. Therefore, water temperatures of both 2 °C and 70 °C could reduce the thickness of the recast layer on the hole sidewall; the recast layer was thinner in 2 °C water.

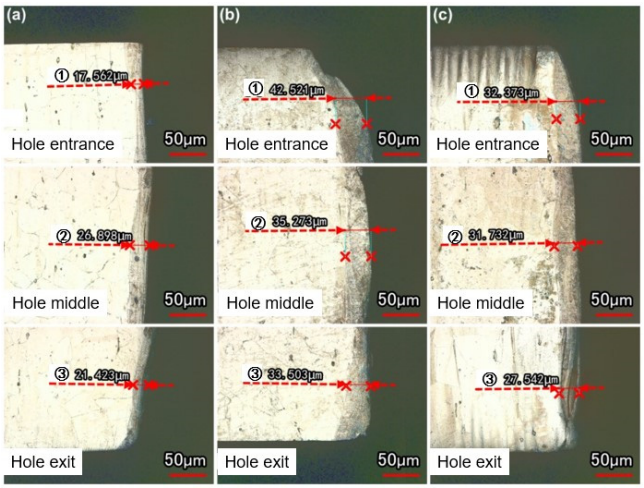

Figure 11. The thickness of the recast layer at different areas of the hole wall at different water temperatures: (**a**) 2 °C, (**b**) 20 °C, and (**c**) 70 °C.

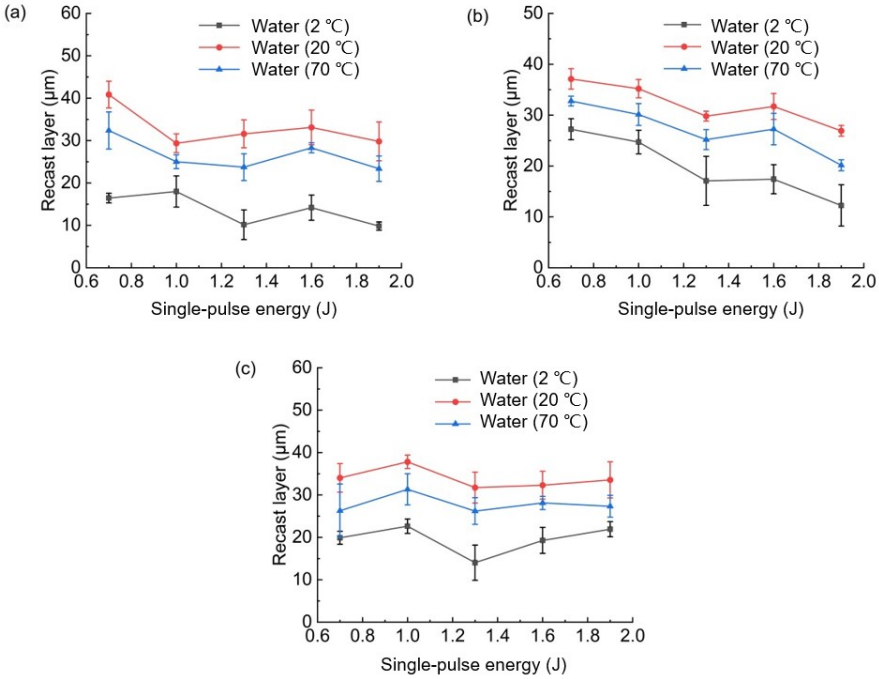

Figure 12. Effect of single-pulse energy on hole recast layer: (**a**) hole entrance; (**b**) hole middle; and (**c**) hole exit.

3.6. Theoretical Analysis

During water-assisted laser trepanning, after the millisecond laser acts on the superalloy, the material continuously melts and evaporates; finally, the majority of the material is removed in the form of spatter. Steam and plasma plumes are generated inside the hole, and the heat-affected zone (HAZ) forms around the hole [27]. After the material is drilled through, water enters the hole. Due to the thermal convection of the movement of water caused by bubbles and the increase in the recoil pressure of the plume in the water [23,28], the material is effectively discharged from the ablation area, and the material removal rate therefore increases [29,30].

Figure 13 shows a schematic diagram of the removal of material at different water temperatures. At the low temperature of 2 °C (Figure 13a), some energy was absorbed by the cold water; as a result, we observed less melt film on the hole sidewall and less formation of bubbles, mixed plumes, and spatter, ultimately leading to a decrease in the hole's diameter and the thickness of the recast layer. At a temperature of 20 °C (Figure 13b), the energy absorbed by the water decreased, resulting in an increase in melt film on the hole sidewall and the formation of more bubbles, mixed plume, and spatter, ultimately leading to an increase in the hole's diameter and the thickness of the recast layer. At the high temperature of 70 °C (Figure 13c), more mixed plumes and spatter were produced, resulting in an increase in bubbles. The thermal convection of the water and the water's movement (caused by the bubbles) were enhanced, and the recoil pressure of the mixed plumes in the water also increased, leading to a decrease in the thickness of the melt film on the hole sidewall and an increase in the hole's diameter. The recast layer was thinner at 70 °C than at 20 °C.

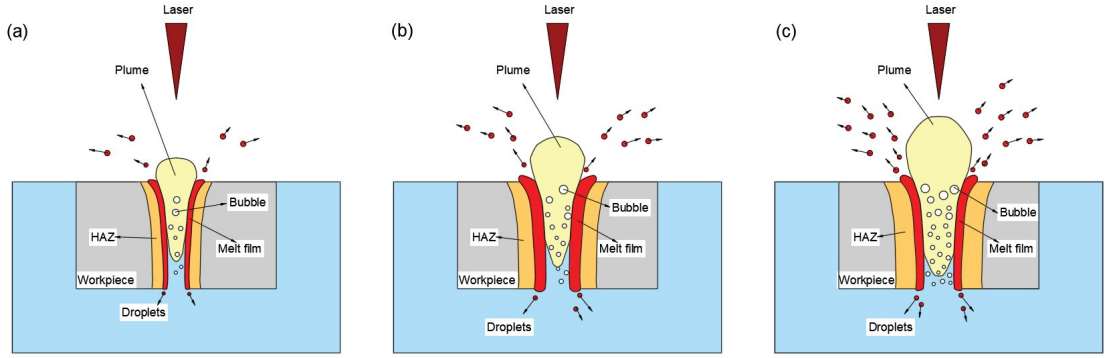

Figure 13. Schematic of water-assisted millisecond laser trepanning: (**a**) 2 °C; (**b**) 20 °C; and (**c**) 70 °C.

4. Conclusions

In this study, we experimentally investigated the effect of water temperature on the quality of holes produced via water-assisted laser trepanning using different laser pulse energies. Therefore, we have provided a reference for the optimization of water-assisted laser drilling. We may draw the following five conclusions:

(1) At different water temperatures, with an increase in laser pulse energy, the spatter around the hole's entrance decreased, the hole entrance and exit diameters increased, and the roughness of the hole's sidewall decreased. Laser pulse energy also had a certain impact on the thickness of the recast layer on the hole's sidewall, but this influence was not obvious.

(2) With an increase in water temperature, the hole entrance and exit diameters increased with the assistance of water. This increase in hole diameter occurred because, when the water temperature was 70 °C, the evaporation of the water medium was more intense; as a result, the spraying of molten materials, debris, and plasma from the hole (generated by laser action) was accelerated. Consequently, the material removal rate improved.

(3) When the single-pulse energy was 0.7 J, the hole taper was at its peak in 2 °C water and reached its minimum in 20 °C water. The amount of water vapor generated via heating was relatively smaller and mainly affected the hole's exit area. The increase in water temperature had a more significant effect on the diameter of the hole's entrance, resulting in an increase in the hole's taper when the single-pulse energy was between 1.0 and 1.9 J.

(4) As the temperature of the water medium increased, the roughness of the hole sidewall decreased. This decrease in roughness occurred because when the water temperature was higher, the water medium and the water vapor generated via heating promoted the removal of molten materials from the hole, resulting in a smoother sidewall.

(5) Compared with 20 °C water, in 70 °C water, the movement of melt film on the hole sidewall accelerated, and more molten material could therefore be removed from the hole, resulting in a decrease in the thickness of the recast layer. However, in 2 °C water, the thermal effect generated during laser drilling decreased; thus, the recast layer thickness decreased more significantly. Therefore, during actual processing, an appropriate water medium temperature should be selected based on the required quality of the hole to be produced, taking into consideration the effects of water temperature on the spatter, hole diameter, taper angle, sidewall roughness, and recast layer.

Author Contributions: Conceptualization, K.X. and L.W.; methodology, K.X., H.Y. and L.W.; validation, K.X. and L.W.; formal analysis, M.L. and H.Y.; investigation, L.W., M.L., H.Y. and K.X.; resources, K.X. and L.W.; data curation, M.L. and H.Y.; writing—original draft preparation, K.X., L.W. and H.Y.; writing—review and editing, K.X. and M.L.; supervision, K.X.; project administration, K.X., M.L. and H.Y.; funding acquisition, K.X. and L.W. All authors have read and agreed to the published version of the manuscript.

Funding: This research was funded by the National Natural Science Foundation of China [grant number 52205469 and grant number 52375434].

Data Availability Statement: The original contributions presented in the study are included in the article, further inquiries can be directed to the corresponding author.

Acknowledgments: We gratefully acknowledge the beneficial discussions and technical support of Jianke Di, Hongmei Zhang, and Naifei Ren.

Conflicts of Interest: Author Kaibo Xia was employed by Jiangsu university and a postdoctoral fellow at the company Suzhou Delphi Laser Co., Ltd., Suzhou, China. The remaining authors declare that the research was conducted in the absence of any commercial or financial relationships that could be construed as a potential conflict of interest.

References

1. Gautam, G.D.; Pandey, A.K. Pulsed Nd: YAG laser beam drilling: A review. *Opt. Lasers Technol.* **2018**, *100*, 183–215. [CrossRef]
2. Gao, L.; Liu, C.; Liu, J.J.; Yang, T.; Jin, Y.; Sun, D. Hole formation mechanisms in double-sided laser drilling of Ti6Al4V-C/SiC stacked materials. *J. Mater. Process. Technol.* **2024**, *325*, 118307. [CrossRef]
3. Zheng, H.Y.; Gan, E.; Lim, G.C. Investigation of laser via formation technology for the manufacturing of high density substrates. *Opt. Laser Eng.* **2001**, *36*, 355–371. [CrossRef]
4. Ho, C.C.; Kao, C.Y. Laser percussion drilling of transparent hard and brittle materials with ring-shaped electrodes. *J. Manuf. Process.* **2023**, *101*, 432–445. [CrossRef]
5. Liang, C.; Li, Z.; Wang, C.; Li, K.; Xiang, Y.; Jia, X.S. Laser drilling of alumina ceramic substrates: A review. *Opt. Lasers Technol.* **2023**, *167*, 109828. [CrossRef]
6. Niu, J.; Yang, J.; Tan, J.Q.; Qin, Z.Y.; Chen, L.; Jia, T.Q.; Xu, H.X. Study of the TBC delamination in nanosecond laser percussion drilling of inclined film cooling holes. *Opt. Lasers Technol.* **2024**, *169*, 110077. [CrossRef]
7. Li, J.C.; Zhang, W.; Zheng, H.Y.; Gao, J.; Jiang, C. Reducing plasma shielding effect for improved nanosecond laser drilling of copper with applied direct current. *Opt. Lasers Technol.* **2023**, *163*, 109372. [CrossRef]
8. Zhang, N.; Wang, M.S.; Ban, M.X.; Guo, L.J.; Liu, W.W. Femtosecond laser drilling 100 μm diameter micro holes with aspect ratios> 20 in a Nickel based superalloy. *J. Mater. Res. Technol.* **2024**, *28*, 1415–1422. [CrossRef]
9. Zhang, T.L.; Yuan, H.; Cai, M. Effects of recast layer on fatigue performance of laser-drilled holes in nickel-based superalloy. *J. Mater. Process. Technol.* **2023**, *311*, 117821. [CrossRef]
10. Ai, S.D.; Xiao, G.J.; Deng, Z.C.; Huang, Y.; Liu, S.; Lin, O.C.; Song, S.Y. Surface integrity of drilling Ti-6Al-4V micro-holes using the ultrashort pulse laser with different three-dimensional paths planning. *J. Manuf. Process.* **2023**, *102*, 244–258. [CrossRef]
11. Goyal, R.; Dubey, A.K. Modeling and optimization of geometrical characteristics in laser trepan drilling of titanium alloy. *J. Mech. Sci. Technol.* **2016**, *30*, 1281–1293. [CrossRef]
12. Wang, M.L.; Yang, L.J.; Zhang, S.; Wang, Y. Experimental investigation on the spiral trepanning of K24 superalloy with femtosecond laser. *Opt. Lasers Technol.* **2018**, *101*, 284–290. [CrossRef]
13. Saini, S.K.; Dubey, A.K. Study of material characteristics in laser trepan drilling of ZTA. *J. Manuf. Process.* **2019**, *44*, 349–358. [CrossRef]
14. Jia, X.S.; Chen, Y.Q.; Wang, H.L.; Zhu, G.Z.; Zhu, X. Experimental study on nanosecond-millisecond combined pulse laser drilling of alumina ceramic with different spot sizes. *Opt. Lasers Technol.* **2020**, *130*, 106351. [CrossRef]
15. Ye, M.Y.; Xiu, H.H.; Thein, C.K.; Jiang, B.Y.; Zhao, Y.J.; Liu, G.Y.; Li, H.N. On the prediction of hole geometry in laser trepanning drilling: A generic 3D analytical model considering drill system structure. *Opt. Lasers Technol.* **2024**, *177*, 111158. [CrossRef]

16. Zhang, Z.; Liu, S.Y.; Zhang, Y.Q.; Wang, C.C.; Zhang, S.Y.; Yang, Z.N.; Xu, W. Optimization of low-power femtosecond laser trepan drilling by machine learning and a high-throughput multi-objective genetic algorithm. *Opt. Lasers Technol.* **2022**, *148*, 107688. [CrossRef]
17. Liu, Y.Z. Coaxial waterjet-assisted laser drilling of film cooling holes in turbine blades. *Int. J. Mach. Tool Manuf.* **2020**, *150*, 103510. [CrossRef]
18. Zhu, S.J.; Zhang, Z.Y.; Chu, S.L.; Yang, Z.Y.; Zhang, X.S.; Wang, A.B. Research and application of massive micropores water-assisted picosecond laser processing technology. *Chin. J. Lasers* **2020**, *47*, 0302002.
19. Chen, Q.; Wang, H.J.; Lin, D.T.; Zuo, F.; Zhao, Z.X.; Lin, H.T. Characterization of hole taper in laser drilling of silicon nitride ceramic under water. *Ceram. Int.* **2018**, *44*, 13449–13452. [CrossRef]
20. Feng, D.C.; Shen, H. Hole quality control in underwater drilling of yttria-stabilized zirconia using a picosecond laser. *Opt. Lasers Technol.* **2019**, *113*, 141–149. [CrossRef]
21. Wang, W.J.; Song, H.W.; Liao, K.; Mei, X.S. Water-assisted femtosecond laser drilling of 4H-SiC to eliminate cracks and surface material shedding. *Int. J. Adv. Manuf. Technol.* **2021**, *112*, 553–562. [CrossRef]
22. Zhang, H.L.; Kang, M.; Ma, C.B.; Mao, Y.; Wang, X.S.; Zhang, Y.N. Experimental investigation and optimization of modification during backside-water-assisted laser drilling using flowing water. *J. Manuf. Process.* **2023**, *101*, 999–1012. [CrossRef]
23. Zhang, H.L.; Mao, Y.; Kang, M.; Ma, C.B.; Li, H.; Zhang, Y.N.; Wang, X.S. Fabrication of high aspect ratio micro-holes on 304 stainless steel via backside-water-assisted laser drilling. *Opt. Lasers Eng.* **2023**, *162*, 107426. [CrossRef]
24. Editorial Committee of China. *Aviation Materials Manual. China Aerospace Materials Handbook*, 2nd ed.; China Standard Press: Beijing, China, 2002; pp. 360–368.
25. Zhang, X.B.; Ji, L.; Cai, M.; Mao, Z.; Li, Y.C.; Zhang, W. Research on ultrafast laser machining of film cooling hole in turbine blade. *Aeronaut. Manuf. Technol.* **2021**, *64*, 14–22.
26. Wang, L.; Yang, H.Y.; Ren, N.F.; Wu, Z.T.; Xia, K.B. Experimental characterization of laser trepanned microholes in superalloy GH4220 with water-based assistance. *Micromachines* **2022**, *13*, 2249. [CrossRef] [PubMed]
27. Zhang, Y.; He, X.L.; Yu, G.; Li, S.X.; Tian, C.X.; Ning, W.J.; Zhang, Y.M. Dynamic evolution of keyhole during multi-pulse drilling with a millisecond laser on 304 stainless steel. *Opt. Lasers Technol.* **2022**, *152*, 108151. [CrossRef]
28. Zhigilei, L.V.; Lin, Z.; Ivanov, D.S. Atomistic modeling of short pulse laser ablation of metals: Connections between melting, spallation, and phase explosion. *J. Phys. Chem. C* **2009**, *113*, 11892–11906. [CrossRef]
29. Behera, R.R.; Sankar, M.R. State of the art on Under Liquid Laser Beam Machining. *Mater. Today Proc.* **2015**, *2*, 1731–1740. [CrossRef]
30. Kruusing, A. Underwater and water-assisted laser processing: Part 2—Etching, cutting and rarely used methods. *Opt. Laser Eng.* **2004**, *41*, 329–352. [CrossRef]